IOP Publishing Superconductor Science and Technology
Supercond. Sci. Technol. 31 (2018) 015011 (15pp) https://doi.org/10.1088/1361-6668/aa9800

Two-band induced superconductivity in single-layer graphene and topological insulator bismuth selenide

E F Talantsev[1], W P Crump[1] and J L Tallon[1,2]

[1] Robinson Research Institute, Victoria University of Wellington, 69 Gracefield Road, Lower Hutt, 5040, New Zealand
[2] MacDiarmid Institute for Advanced Materials and Nanotechnology, PO Box 33436, Lower Hutt 5046, New Zealand

E-mail: evgeny.talantsev@vuw.ac.nz

Received 12 July 2017, revised 28 October 2017
Accepted for publication 3 November 2017
Published 29 November 2017

Abstract

Proximity-induced superconductivity in single-layer graphene (SLG) and in topological insulators represent almost ideal examples of superconductivity in two dimensions. Fundamental mechanisms governing superconductivity in the 2D limit are of central interest for modern condensed-matter physics. To deduce fundamental parameters of superconductor/graphene/superconductor and superconductor/bismuth selenide/superconductor junctions we investigate the self-field critical currents in these devices using the formalism of the Ambegaokar–Baratoff model. Our central finding is that the induced superconducting state in SLG and bismuth selenide each exhibits gapping on two superconducting bands. Based on recent results obtained on ultra-thin films of natural superconductors, including single-atomic layer of iron selenide, double and triple atomic layers of gallium, and several atomic layer tantalum disulphide, we conclude that a two-band induced superconducting state in SLG and bismuth selenide is part of a wider, more general multiple-band phenomenology of currently unknown origin.

Supplementary material for this article is available online

Keywords: graphene, bismuth selenide, Josephson junction, Ambegaokar–Baratoff model, superconducting gap, Josephson current

(Some figures may appear in colour only in the online journal)

1. Introduction

Fundamental mechanisms governing induced superconductivity in two-dimensional (2D) materials [1–9] and topological insulators [10, 11] represent a current and very active research topic in physics. In this paper we analyze experimental self-field critical currents, I_c(sf, T), reported in the literature in superconductor/graphene/superconductor (S/G/S) and superconductor/topological insulator/superconductor (S/TI/S) junctions using the Ambegaokar–Baratoff (A–B) equation [12, 13]. To fit experimental I_c(sf, T) datasets to the A–B equation we use an analytical expression for the temperature-dependent gap equation given by Gross *et al* [14]. As a result of this approach, we deduced three fundamental superconducting parameters of the junction, i.e., the transition temperature, T_c, the ground-state amplitude of the superconducting gap, $\Delta(0)$, and the relative jump in electronic specific heat, $\Delta C/C$, at the transition temperature. To our knowledge this approach was not described previously.

The main result of our analysis is that induced superconductivity in single-layer graphene (SLG) and the three-dimensional topological insulator, bismuth selenide (Bi_2Se_3),

both surprisingly have two active bands with distinct superconducting gaps.

2. Model description

Ambegaokar and Baratoff [12, 13] developed an approach to describe self-field critical currents, $I_c(sf, T)$, in Josephson junctions [15]. The simplest analytical expression of the model is given by the following equation:

$$I_c(T) = \frac{\pi\Delta(T)}{2eR_n} \cdot \tanh\left(\frac{\Delta(T)}{2k_BT}\right), \quad (1)$$

where e is the electron charge, R_n is the normal-state tunneling resistance in the junction, and k_B is the Boltzmann constant. One of the most useful and robust analytical expressions for the temperature-dependent superconducting gap, $\Delta(T)$, which allows variable coupling strength of the electron-boson interaction, was given by Gross *et al* [14]:

$$\Delta(T) = \Delta(0) \cdot \tanh\left(\frac{\pi\, k_B\, T_c}{\Delta(0)} \cdot \sqrt{\eta\left(\frac{\Delta C}{C}\right)\left(\frac{T_c}{T} - 1\right)}\right), \quad (2)$$

where $\Delta(0)$ is the ground-state amplitude of the superconducting band, $\Delta C/C$ is the relative jump in electronic specific heat at the transition temperature, T_c, and $\eta = 2/3$ for s-wave superconductors [14]. Thus, by substituting equation (2) in (1) (which is given below in full form):

$$I_c(T) = \frac{\pi \cdot \Delta(0) \cdot \tanh\left(\frac{\pi\, k_B\, T_c}{\Delta(0)} \cdot \sqrt{\eta\left(\frac{\Delta C}{C}\right)\left(\frac{T_c}{T} - 1\right)}\right)}{2eR_n} \cdot \tanh\left(\frac{\Delta(0) \cdot \tanh\left(\frac{\pi\, k_B\, T_c}{\Delta(0)} \cdot \sqrt{\eta\left(\frac{\Delta C}{C}\right)\left(\frac{T_c}{T} - 1\right)}\right)}{2k_BT}\right) \quad (3)$$

we have a tool to deduce the fundamental superconducting parameters T_c, $\Delta C/C$ and $\Delta(0)$ by fitting experimental self-field $I_c(sf, T)$ datasets to equation (3).

To our knowledge, the substitution of the analytical gap equation of Gross *et al* [14] (equation (2)) in the A–B equation (1) and the consequent deduction of junction superconducting parameters was not reported before. Probably the main reason for this is that several alternative models that employed the detailed band structure to describe $I_c(T)$ were developed beyond the A–B model, of which we can mention the well-known works of Likharev [16], and Kulik and Omelyanchuk [17]. Detailed reviews of alternative models beyond the A–B model are given in Delin and Kleinsasser [18] and Golubov *et al* [19]. More recently, for a fuller description of superconducting transport in Josephson junctions with a barrier of graphene or topological insulator several other theoretical models were employed (for instance, Eilenberger [20], Usadel [21], Brinkman and Golubov [22]), and some new theoretical approaches were developed [23].

However, the A–B model is still the basic, simplest and most widely-used model to analyze Josephson currents, including in superconducting cuprates [24, 25]. For example, this model is the standard model to describe c-axis superconducting currents in cuprates, since Kleiner *et al* [26] showed that the A–B model works quite well. Despite the fact that the single junction length in cuprates, for instance in $Bi_2Sr_2CaCu_2O_8$, is in the short limit, for single crystals with thickness of $L = 20$–$50\ \mu$m the number of series junctions exceeds 10 000. As noted, Kleiner *et al* [26, 27] found that the experimental $I_c(T)$ is described quite well by the A–B model. This was then confirmed by many studies over two decades [28–30]. Recently, the A–B model was also applied to the analysis of c-axis superconducting transport in pnictide superconductors [31].

For these reasons we have restricted our considerations here to the Ambegaokar and Baratoff [12, 13] model with the purpose of showing that an induced superconducting state in graphene and topological insulators Bi_2Se_3 gap on two superconducting bands. A more complete description of $I_c(T)$ where the detailed band structure must be considered can follow from this work including refinements to address the long junctions considered later in this paper. However, the main physical result we are reporting here (i.e. two-band induced superconductivity in graphene and the topological insulator Bi_2Se_3) is robust even in the absence of these refinements. We will show that our straightforward approach is a convenient and instructive starting point which enables deduction of the fundamental parameters of the junction. As a first step we will demonstrate that our approach works well for classical junctions and after that we will consider Josephson junctions where weak-links were made using graphene or the topological insulator, Bi_2Se_3.

Experimental data analyzed in this paper was obtained by digitizing figures in the original research papers with one exception for the MoRe/SLG/MoRe junction [3], for which the raw $I_c(sf, T)$ dataset was provided by Dr S Goswami and Professor L M K Vandersypen (Kavli Institute of Nanoscience, Delft University of Technology, The Netherlands).

3. Results

3.1. Junctions beyond graphene

To demonstrate how our approach works to deduce T_c, $\Delta C/C$, and $\Delta(0)$ values for classical junctions, in figures 1–3 we present experimental self-field $I_c(sf, T)$ datasets and their fits to equation (3). As the $I_c(sf, T)$ analysis and the full description of all junctions considered herein were given in the original reports, we do not repeat this information here (for instance, the effective junction length, L/ξ, the junction width, W/ξ, etc) because these parameters can be found in the original papers. We only indicate the geometrical (physical) length of the junction, L, herein.

3.1.1. Sn/SnO$_x$/Sn junction; L ∼ several Å. In figure 1(a) we show the $I_c(sf, T)$ dataset for a Sn/SnO$_x$/Sn junction from the classic paper of Anderson and Goldman [32] and its fit using equation (3). The deduced parameters are remarkably close to the weak-coupling limit for a BCS superconductor. Indeed,

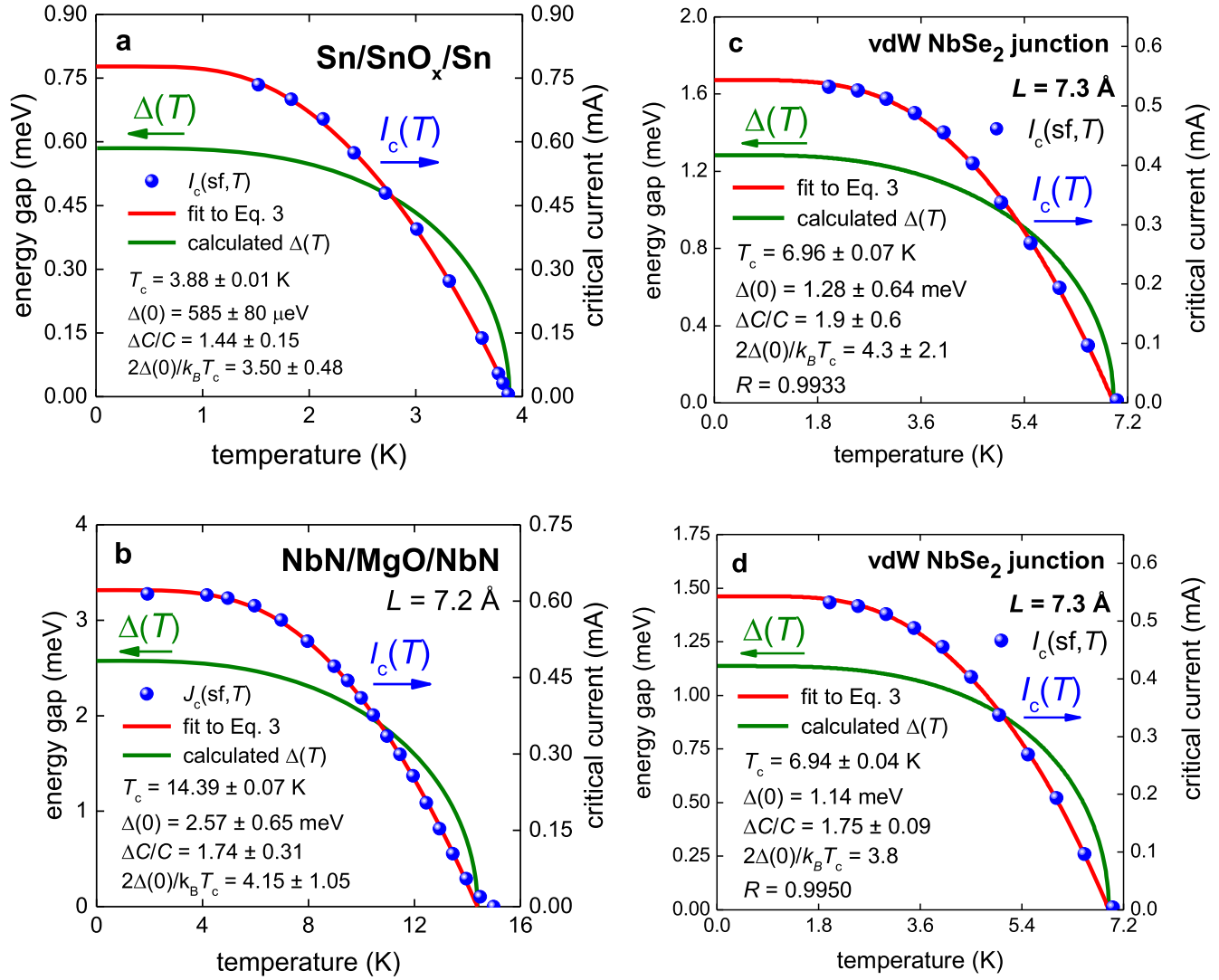

Figure 1. Experimental I_c(sf, T) datasets and fits to equation (3) together with the calculated $\Delta(T)$ for several short junctions. (a) Sn/SnO$_x$/Sn junction (L is several Å) (experimental data from [32]). $R_n = 1.18 \pm 0.17\,\Omega$, $R_{n,exp} = 1.0\,\Omega$. The goodness-of-fit quality is $R = 0.9909$. (b) NbN/MgO/NbN junction ($L = 7.2$ Å) (experimental data from [36]). The goodness-of-fit quality is $R = 0.9974$. (c), (d) The van der Waals coupled $NbSe_2$ Josephson junction ($L = 7.3$ Å) (experimental data from [40]). In panel (c) all model parameters are free. $R_n = 3.7 \pm 1.8\,\Omega$, $R_{n,exp} = 1.97\,\Omega$, with a goodness-of-fit quality given by $R = 0.9933$. In panel (d) the model was restricted by fixing $2\Delta(0)/k_BT_c = 3.8$. $R_n = 3.29 \pm 0.02\,\Omega$, $R_{n,exp} = 1.97\,\Omega$, and the fit quality is $R = 0.9950$.

the deduced energy gap, $\Delta(0) = 0.585 \pm 0.080$ meV, is in remarkably good agreement with the independently-reported value, $\Delta(0) = 0.593$ meV, given by Wolf [33]. Lower temperature data below $T = 1.5$ K would significantly reduce the uncertainties quoted here. The inferred BCS ratio of $2\Delta(0)/k_BT_c = 3.50 \pm 0.48$ is again in good accord with the BCS weak-coupling limit of 3.52 [34].

We note that Padamsee and coworkers [35], using their so-called α-model for general coupling strength, deduced from the temperature dependence of the critical field for Sn that $\Delta(0)/k_BT_c = 1.88$, in good agreement with our inference of near-weak-coupling behavior. The deduced relative specific heat jump, $\Delta C/C = 1.44 \pm 0.15$, is also consistent with the BCS weak-coupling limit of 1.43 [14]. Finally, the deduced normal-state tunneling resistance $R_n = 1.18 \pm 0.17\,\Omega$ agrees well with the experimentally-measured value of $R_{n,exp} = 1.0\,\Omega$.

3.1.2. NbN/MgO/NbN junction; L = 7.2 Å. To show further that our approach also reliably deduces T_c, $\Delta C/C$, and $\Delta(0)$ for strong-coupling superconductors, we show in figure 1(b) experimental I_c(sf, T) datasets for the NbN/MgO/NbN junction reported by Shoji *et al* [36] together with the fit to equation (3).

Our deduced values for the BCS ratio, $2\Delta(0)/k_BT_c = 4.15 \pm 1.05$, and for the relative specific heat jump at transition temperature, $\Delta C/C = 1.74 \pm 0.31$, again are in excellent agreement with the reported measurements for these quantities, $2\Delta(0)/k_BT_c = 4.25$ [37] and $\Delta C/C = 1.90 \pm 0.09$ [38].

Thus, we can conclude that our model (equation (3)) successfully derives thermodynamic parameters for short junctions in the case of moderately strong-coupling superconductors and it does not restrict to just the weak-coupling BCS limit.

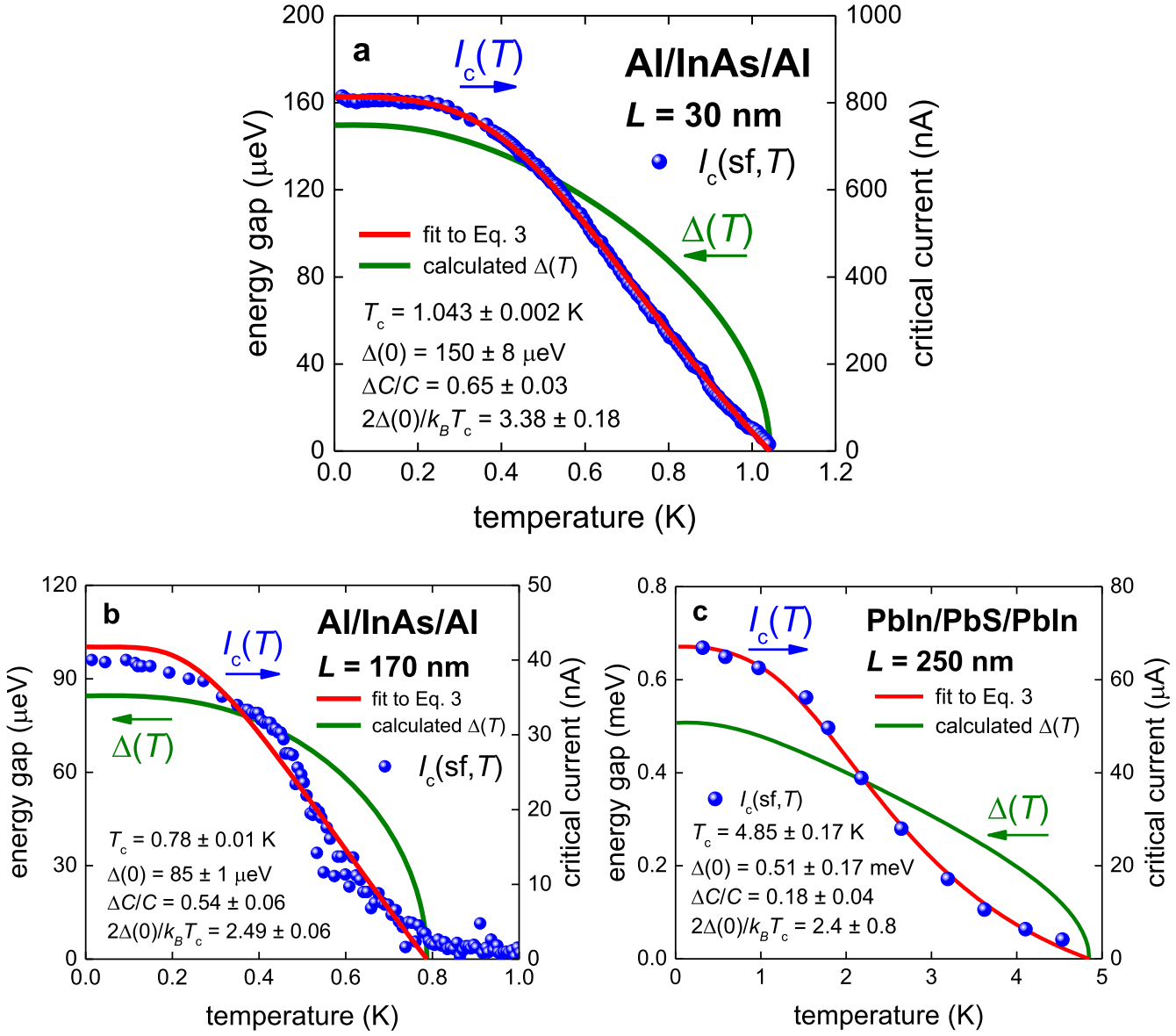

Figure 2. Experimental I_c(sf, T) dataset and fit to equation (3) for long junctions Al/InAs/Al junctions together with calculated $\Delta(T)$. (a) Al/InAs/Al ($L = 30$ nm) (experimental data from [39]); $R_n = 289 \pm 15\,\Omega$, $R_{n,exp} = 160\,\Omega$, fit quality is $R = 0.9996$. (b) Al/InAs/Al ($L = 170$ nm) (experimental data from [39]); $R_n = 2.9 \pm 0.4\,k\Omega$, $R_{n,exp} = 1.28\,k\Omega$, fit quality is $R = 0.9530$. (c) PbIn/PbS/PbIn ($L = 250$ nm) (experimental data from [47]); $R_n = 1.3 \pm 0.4\,k\Omega$, fit quality is $R = 0.9515$.

We should note three issues. One is that our main goal is to study induced superconductivity in graphene and topological insulators. To simplify the task, we only analyze I_c(sf, T) datasets for junctions that have the same superconducting materials for both electrodes.

The second is that for all fits presented in this paper, we keep R_n in equation (3), as a free-fitting parameter. The reason for this is that experimentally-measured $R_{n,exp}$ values even for nominally identical junctions manufactured by the same technology can be variable within a quite large span [39]. As the A–B model (equation (1)) describes the ideal junction, to fix the R_n value to $R_{n,exp}$ and fit experimental I_c(sf, T) datasets to equation (3) may not always be appropriate. Instead, in this paper we allow the R_n parameter to be free and, after the fit convergence, we compare the derived R_n value with the experimentally-measured, $R_{n,exp}$. In most studied cases $R_{n,exp} < R_n$, however some junctions showed $R_{n,exp} > R_n$. The particular reason for these variations is not clear but some of the issues are discussed in [39]. In this paper we simply list both values in the figure captions.

The third is that, if the experimental I_c(sf, T) dataset is not rich enough (i.e. extending in close intervals from T_c to lower than 0.15 T_c) then fits often reveal a high 'mutual parameters dependence' (the definition of mutual parameter dependence is given in the supplementary information which is available online at stacks.iop.org/SUST/31/015011/mmedia) with resulting large uncertainties in the derived parameters. To illustrate this, in figures 1(c) and (d) we show an I_c(sf, T) dataset reported by Yabuki *et al* [40] and fit for a van der Waals coupled Josephson junction made of two exfoliated

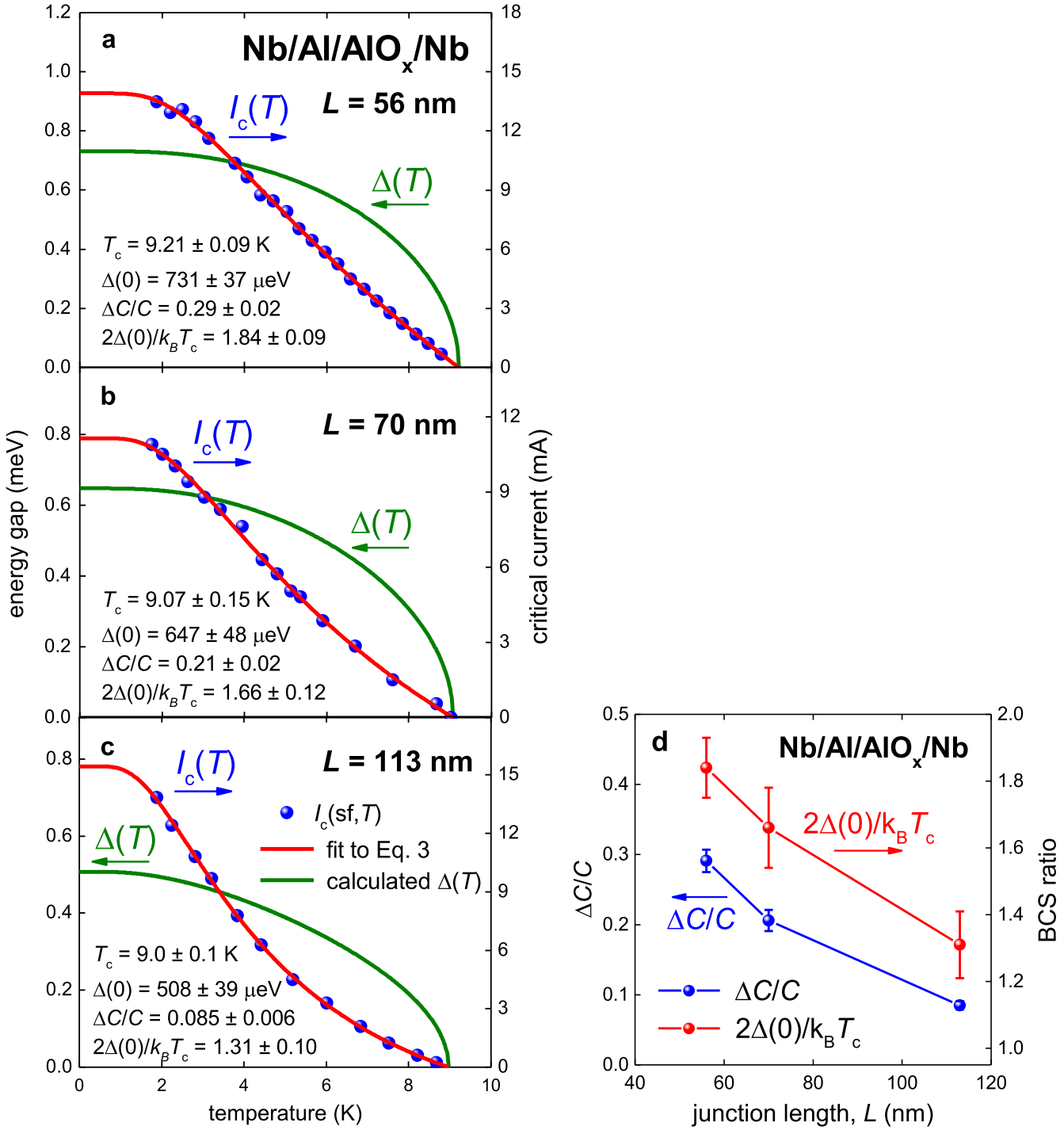

Figure 3. Experimental I_c(sf, T) data from [48] and fits to equation (3) for Nb/Al/AlO$_x$/Nb junctions together with calculated $\Delta(T)$. (a) $L = 56$ nm. $R_n = 83 \pm 5$ mΩ, fit quality is $R = 0.9939$; (b) $L = 70$ nm. $R_n = 91 \pm 8$ Ω, fit quality is $R = 0.9865$; (c) $L = 113$ nm. $R_n = 52 \pm 5$ mΩ, fit quality is $R = 0.9912$; (d) dependences of $\Delta C/C$ and $2\Delta(0)/k_BT_c$ on junction length, L.

niobium dichalcogenide, $NbSe_2$, crystals with estimated junction length of $L = 7.3$ Å [40].

3.1.3. van der Waals $NbSe_2$ junction; $L = 7.3$ Å. Panel (c) in figure 1 represents the fit for which all parameters were free. Despite the fact that the derived parameters concur well with expected values ($NbSe_2$ is a moderately strong-coupling superconductor), and the goodness-of-fit parameter $R = 0.9933$, is high, it can be seen that uncertainties for the derived parameters are as high as 50%. This is an indication that the I_c(sf, T) dataset is not rich enough to deduce the three superconducting parameters with acceptable accuracy. We still can analyze the data, but the number of free-fitting parameters should be reduced. This reduction should be based on some reasonable assumption.

Let us show how this can be done by making two different assumptions. First, in figure 1(d) we show the fit for

which $2\Delta(0)/k_BT_c$ was fixed to 3.8. This value was chosen based on the upper limit for $\Delta(0) = 1.2$ meV recently reported for $NbSe_2$ crystals by Weber *et al* [41], and taking into account that a similar value $\Delta(0) = 1.24 \pm 0.04$ meV was reported by Morris and Coleman [42] in the early 1970s. For this restricted-fit model the goodness of fit $R = 0.9950$ (see $R = 0.9933$ for figure 1(c)) and the difference in I_c(sf, T) fitting curves in panels (c) and (d) is not discernible. However, as can be seen the uncertainty for $\Delta C/C$ was reduced significantly.

The second assumption is based on analyzing the dI/dV versus V plot presented in figures 3(a), (b) of [40]. We digitized figure 3(b) and perform the fit of the digitized dataset to the gap equation of Gross *et al* [14] (equation (2)). The fit is shown in supplementary information figure S1. The deduced parameters are: $T_c = 6.84 \pm 0.04$ K, $\Delta(0) = 0.773 \pm 0.006$ meV, $\Delta C/C = 0.98 \pm 0.06$, $2\Delta(0)/k_BT_c = 2.62 \pm 0.04$. We note that the transition temperature, the energy gap amplitude and the BCS ratio are, within the fitting uncertainties, in good agreement with values deduced by the A–B equation (3) presented in figure 1(c) where all parameters were free.

Now we can restrict the BCS gap ratio to the value of $2\Delta(0)/k_BT_c = 2.62$ and perform the I_c(sf, T) fit again. The result is shown in figure S2 of supplementary information. Deduced parameters are: $T_c = 6.84 \pm 0.09$ K, $\Delta(0) = 0.773 \pm 0.010$ meV, $\Delta C/C = 1.54 \pm 0.24$, the goodness of fit $R = 0.9885$ (which is lower than that for figures 1(c), (d)). However, again, within fitting uncertainties the derived values agree with values deduced by the A–B equation (3) presented in figure 1(c), when all parameters were left free.

This example demonstrates that the I_c(sf, T) experimental datasets should be rich and wide enough to deduce the superconducting parameters of the studied junction with high robustness and accuracy.

3.1.4. Al/InAs/Al; L = 30, 170 nm. The Al/InAs nanowire/Al junction system has been studied extensively [39, 43–45]. From a variety of available I_c(sf, T) datasets we present in figures 2(a) and (b) the two most rich datasets and their corresponding fits for Al/InAs/Al junctions with lengths of $L = 30$ nm and $L = 170$ nm reported by Abay *et al* [39] in their figure 8.

The derived parameters for these two junctions show that for the shorter junction, $L = 30$ nm, the derived BCS ratio $2\Delta(0)/k_BT_c = 3.38 \pm 0.18$ still can be considered to be within the range of the weak-coupling limit for Al (see, figure 1(a) for weak-coupled tin in $Sn/SnO_x/Sn$ junction). But for the longer junction $L = 170$ nm the derived ratio $2\Delta(0)/k_BT_c = 2.49 \pm 0.06$ is clearly well below the weak-coupling limit.

Also we found that even for the shorter junction the derived value for $\Delta C/C = 0.65 \pm 0.03$ falls significantly below the weak-coupling limit of 1.43. This marked reduction in $\Delta C/C$ for moderately long junctions was also observed in other Al/InAs/Al junctions and this signals an important change in the physics of longer junctions.

3.1.5. PbIn/PbS/PbIn; L = 250 nm. We analyzed in figure 1(b) the supercurrent in a short Josephson junction made of moderately strong-coupled NbN. Now we show that our model can be applied for a long Josephson junction, $L = 250$ nm, made of the moderately strong-coupled superconducting alloy PbIn [46]. Kim *et al* [47] in their figure 2(b) reported I_c(sf, T) datasets for PbIn/PbS-nanowire/PbIn, which we show in figure 2(c) together with the fit to our model.

As already shown in figures 2(a) and (b) when the junction length becomes too long the superconductivity weakens, which is also demonstrated in figure 2(c), where all deduced superconducting parameters are reduced below typical values for weak-link free strong-coupling superconductors. A schematic representation of a simple model which describes this behavior is shown in figure S3, where the color intensity represents the magnitude of the order parameter, ψ, which because of pair-breaking scattering events becomes smaller in the center as L is increased.

3.1.6. Nb/Al/AlO$_x$/Nb; L = 56, 70 and 113 nm. To further illustrate the trend of weakening superconductivity while junction length, L, increases, in figure 3 we show our analysis of I_c(sf, T) datasets reported by Lacquaniti *et al* [48] in their figure 4 for Nb/Al/AlO_x/Nb junctions with $L = 56$, 70 and 113 nm. In figure 3(d) we plot dependences of the derived values of $\Delta C/C$ and $2\Delta(0)/k_BT_c$ on junction length, L. These parameters fall with increasing junction length due to the decay of the order parameter in the junction.

Figures 2 and 3 show a characteristic trend with increasing junction length namely the development of a distinct sigmoidal shape in I_c(sf, T) that renders a distinctly non-canonical shape to $\Delta(T)$. Our fit parameters have characterized this as a weakening of superconductivity and surely this is part of the picture but it is weakening in a distinctive fashion that renormalizes the T-dependence and absolute value of $\Delta(T)$.

The primary physical reason for this is the scattering in the junction, which leads to the distinctive sigmoidal shape of I_c(sf, T) and the non-canonical shape of $\Delta(T)$. In the spirit of Abrikosov–Gorkov (A–G) pair-breaking [49] the important parameter is $\Gamma/\Delta(T)$ where Γ is the scattering rate in the junction material. In the graphene examples (discussed in the next section) this scattering rate is very large for vertical junctions which leads to an extremely short mean-free path and rapid change in I_c(sf, T) as the junction length increases.

For planar single graphene-layer junctions the scattering is very small and leads to an extremely long mean-free path and a slow change in the shape of the temperature dependence of I_c(sf, T) even for junctions with length of 1.5 μm.

Thus, close to T_c where $\Delta(T)$ is small the impact of this scattering is large since $\Gamma/\Delta(T)$ is large and there is a marked suppression of the critical current. But at lower temperatures $\Gamma/\Delta(T)$ is smaller and the impact of scattering is diminished

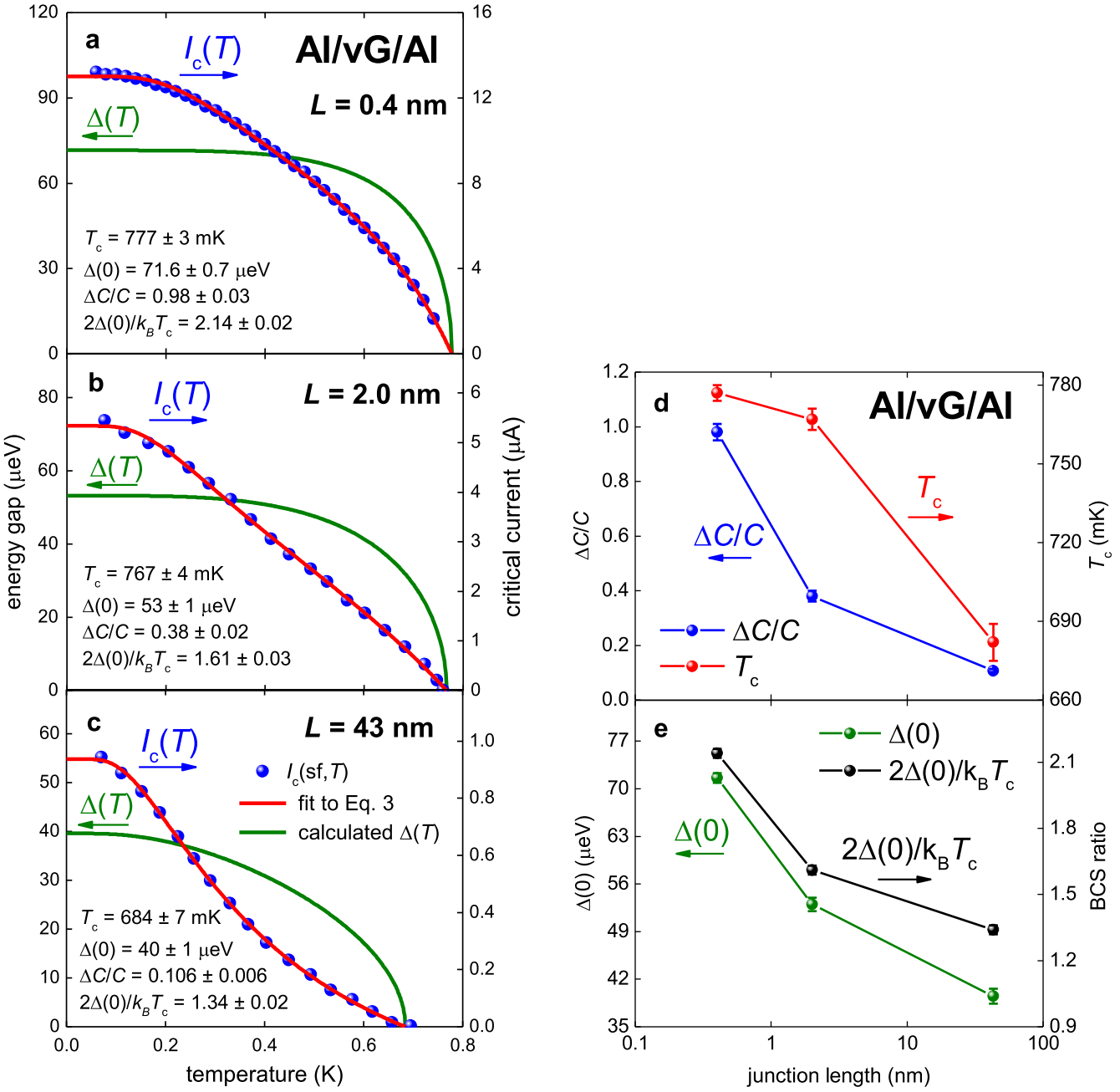

Figure 4. Experimental I_c(sf, T) data from [4] and fits to equation (3) for Al/vG/Al junctions together with calculated $\Delta(T)$. (a) $L = 0.4$ nm. $R_n = 8.64 \pm 0.09\ \Omega$, fit quality is $R = 0.9993$. (b) $L = 2.0$ nm. $R_n = 15.6 \pm 0.5\ \Omega$, fit quality is $R = 0.9925$. (c) $L = 43$ nm. $R_n = 66 \pm 2\ \Omega$, fit quality is $R = 0.9962$. (d) Dependence of T_c and $\Delta C/C$ on junction length. (e) Dependence of $\Delta(0)$ and $2\Delta(0)/k_BT_c$ for junctions length. Note that plots in (d) and (e) are in log-linear scale.

so $I_c(T)$ rises more steeply with decreasing temperature. A more detailed analysis, including extracting the scattering rate, Γ, would not be appropriate in the present work.

3.2. Graphene-based junctions

We turn now to graphene-based junctions. Superconductivity in planar graphene-based Josephson junctions is induced by varying the gate voltage V_g that changes the doping state, n, of the graphene, thereby moving away from the Dirac point in the dispersion. Details can be found elsewhere [3, 5, 9]. We analyze below the available I_c(sf, T) datasets for vertical-junction geometry (vG) and planar-junction geometry where weak-links were created using single and multiple layer(s) of graphene/graphite.

3.2.1. Vertical Al/vG/Al junctions; $L = 0.4$, 2.0, 43 nm. A nice demonstration of gradual reduction of junction superconducting parameters by the local suppression of the order parameter, ψ, as the junction length, L, increases is presented in figure 4, where I_c(sf, T) datasets and fits for three vertical graphene/graphite-based junctions with junction length of $L = 0.4$, 2.0 and 43 nm (which corresponds to SLG, five-layer graphene, and

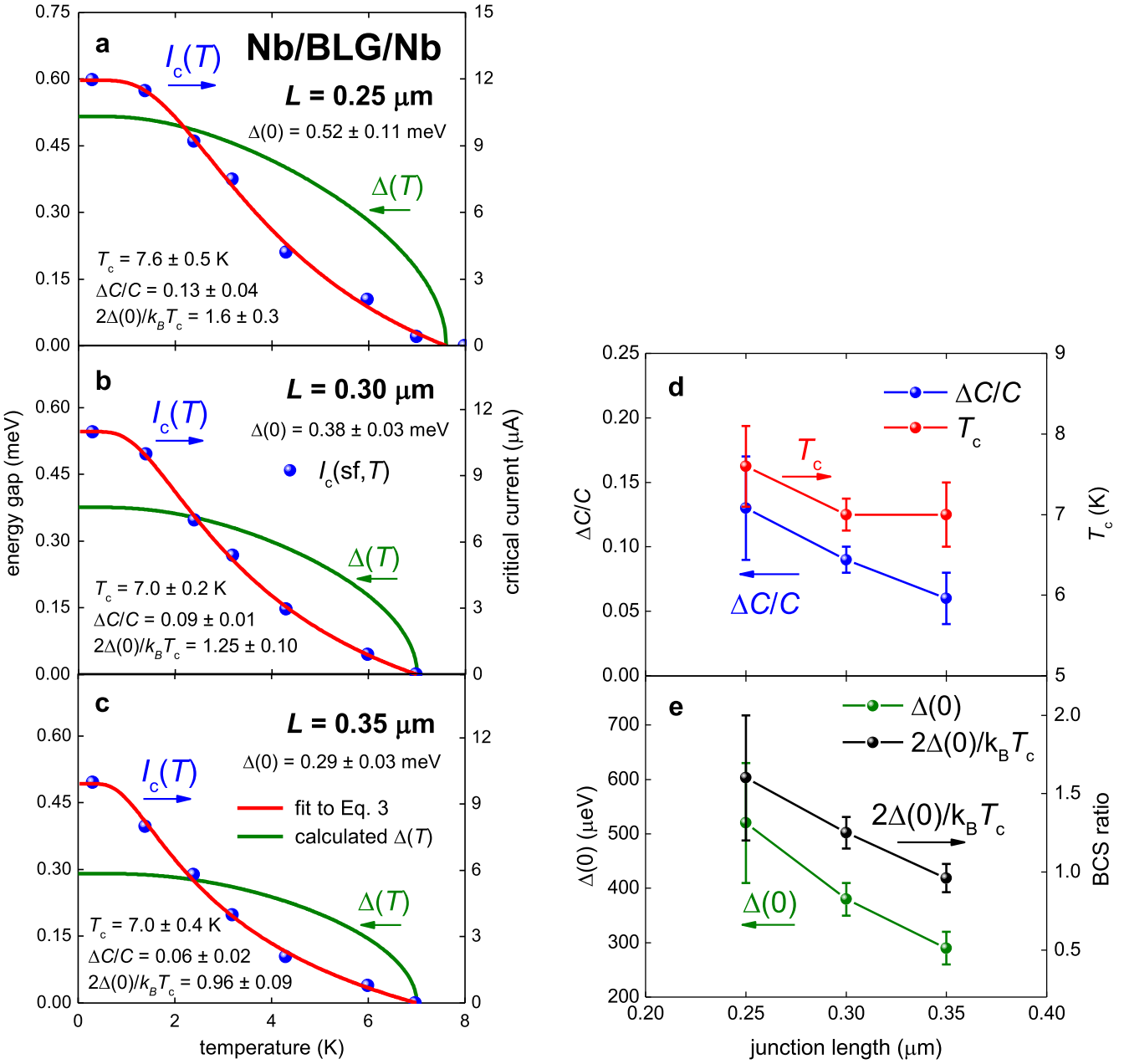

Figure 5. Experimental I_c(sf, T) data from [5] and fits to equation (3) for Nb/BLG/Nb junctions together with calculated $\Delta(T)$ $V_g = 60$ V. (a) $L = 0.25$ μm. $R_n = 68 \pm 16\ \Omega$, fit quality is $R = 0.8865$. (b) $L = 0.30$ μm. $R_n = 54 \pm 5\ \Omega$, fit quality is $R = 0.9452$. (c) $L = 0.35$ μm. $R_n = 46 \pm 5\ \Omega$, fit quality is $R = 0.8234$. (d) Dependence of T_c and $\Delta C/C$ versus the junction length. (e) $\Delta(0)$ and $2\Delta(0)/k_BT_c$ versus the junction length.

a 43 nm graphite flake) are shown for the experimental datasets reported by Lee *et al* [4] in their figure 3(b).

In figures 4(d) and (e) we plot (in log-linear scale) the dependence of the derived parameters, T_c, $\Delta(0)$ and $\Delta C/C$, on junction length, L. For longer junctions the latter two parameters become a proxy for additional junction features beyond the simple A–G picture including multiple Andreev reflection and scattering processes within the tunnel barrier, and the apparent reduction in these parameters will reflect these processes.

To the authors' knowledge the data of Lee *et al* [4] (shown in figure 4) represent the largest variation in junction length available in the literature. Deduced parameters shown in figures 4(d), (e) demonstrate smoothly the progressive weakening of superconductivity with increasing junction length. It can be seen that the transition temperature, T_c, is the least affected parameter while junction length increases. However, other superconducting parameters, $\Delta C/C$ and $2\Delta(0)/k_BT_c$ fall dramatically with increasing junction length. This is due to the exponential decay of the proximity-induced superconductivity in the junction arising from scattering, small or large as it may be. Thus, further development of the model requires extended experimental I_c(sf, T) datasets with smooth variation of junction length from sub-nanometer up to several microns.

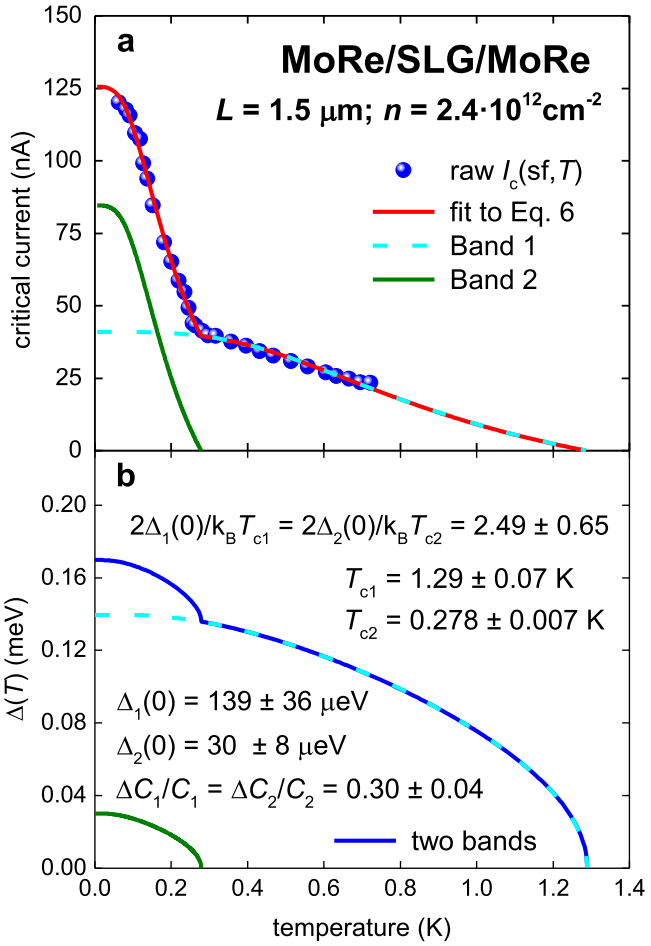

Figure 6. (a) Experimental I_c(sf, T) data from [3] and corresponding fit to the two-decoupled-bands model for a MoRe/SLG/MoRe junction (length of $L = 1.50$ μm) together with (b) calculated $\Delta(T)$. Because of the incomplete dataset the fit was restricted to $2\Delta_1(0)/k_BT_{c1} = 2\Delta_2(0)/k_BT_{c2}$ and $\Delta C_1/C_1 = \Delta C_2/C_2$ to reduce the number of fit parameters. $R_{n1} = 5.3 \pm 1.4$ kΩ, and $R_{n2} = 0.56 \pm 0.16$ kΩ. Fit quality is $R = 0.9876$.

3.2.2. Planar Nb/BLG/Nb; L = 0.25, 0.30, and 0.35 μm. Ben Shalom *et al* [5] reported self-field critical currents, I_c(sf, T), for planar Josephson junctions with niobium electrodes and different junctions lengths of $L = 0.25$, 0.30, 0.35, 0.40 and 0.50 μm. These junctions were made on the same bilayer graphene (BLG) flake. I_c(sf, T) datasets at $V_g = 60$ V are reported in figure S4(b) of [5]. For junctions with lengths of $L = 0.40$ and 0.50 μm, reported I_c(sf, T) datasets were not rich enough to perform the fit to equation (3).

Thus, in figures 5(a)–(c) we only show processed data and fits for three junctions with $L = 0.25$, 0.30, and 0.35 μm. In spite of the relatively large uncertainties for the derived parameters due to the sparse experimental I_c(sf, T) datasets, the trends in figures 5(d), (e) are the same, as we already found for S/N/S junctions (figures 2–4), i.e., the weakening of superconductivity with increasing junction length, L. And again, T_c was found to be the least affected parameter.

Recently, Natterer *et al* [50] performed scanning tunneling spectroscopy measurements of the superconducting energy gap as function of the distance from the edge of superconducting aluminum in Al/multilayer graphene junction. They found an exponential suppression of the gap amplitude. Our result presented in figure 5 is in qualitative agreement with this though more raw data is required to deduce the characteristic length for the suppression.

3.2.3. Planar MoRe/SLG/MoRe; L = 1.5 μm. Calado *et al* [3] reported self-field critical currents, I_c(sf, T), measured by standard d.c. four-point geometry for several MoRe/graphene/MoRe devices with very long junction lengths, $L \geqslant 1.0$ μm. These devices were fabricated from SLG flakes and experimental I_c(sf, T) were measured at different induced carrier concentrations, n.

Figure 6 shows the raw I_c(sf, T) dataset for Device A with $L = 1.5$ μm (figure S1(c) of [3]) where at the applied gate voltage the induced carrier concentration was $n = 2.4 \times 10^{12}$ cm^{-2}. This experimental data reveals a large sharp rise in I_c(sf, T) at temperatures below 300 mK which remains to be explained.

Our approach to explain this result and deduce the associated fundamental superconducting parameters for this junction is based on the recent finding of Talantsev *et al* [51] where the opening of an additional superconducting gap was found in superconductors where the thickness is reduced below the out-of-plane coherence length. Talantsev *et al* [51] demonstrated this for several atomically-thin superconductors, for instance FeSe [52], TaS_2 [53], double and triple atomic layer Ga [54, 55] and thin Nb films [56].

To identify the opening of an additional superconducting gap these authors analyzed the self-field critical current densities, J_c(sf, T), using a model for two completely decoupled bands with:

$$J_{c,\text{total}}(sf, T) = J_{c,1}(sf, T) + J_{c,2}(sf, T), \tag{4}$$

where the subscripts 1 and 2 refer to each band, respectively, and each band has independent fundamental superconducting parameters.

We assume that the same effect of opening a new superconducting band [51] plays a role in proximity-induced superconductivity in SLG-devices as the SLG thickness is atomically thin and certainly less than the coherence length. Thus, we fit the experimental self-field I_c(sf, T) of the MoRe/SLG/MoRe junction reported by Calado *et al* [3] to this two-decoupled-bands model, which in terms of the A–B formalism, is:

$$\begin{aligned} I_{c,\text{total}}(T) &= I_{c,1}(T) + I_{c,2}(T) \\ &= \sum_{n=1}^{2} \frac{\pi\,\Delta_i(T)}{2eR_{n,i}} \cdot \tanh\left(\frac{\Delta_i(T)}{2k_BT}\right), \end{aligned} \tag{5}$$

where the critical current, $I_{c,i}(T)$, of each band is described by equations (1) and (2), and T_{ci}, $\Delta C_i/C_i$, $\Delta_i(0)$, and $R_{n,i}$ are free-fitting parameters of the model. As a consequence of this, the I_c(sf, T) dataset needs to be reasonably rich to derive eight free parameters with acceptable uncertainty and mutual independence. Unfortunately, the I_c(sf, T) dataset reported by Calado *et al* [3] was limited to temperatures below

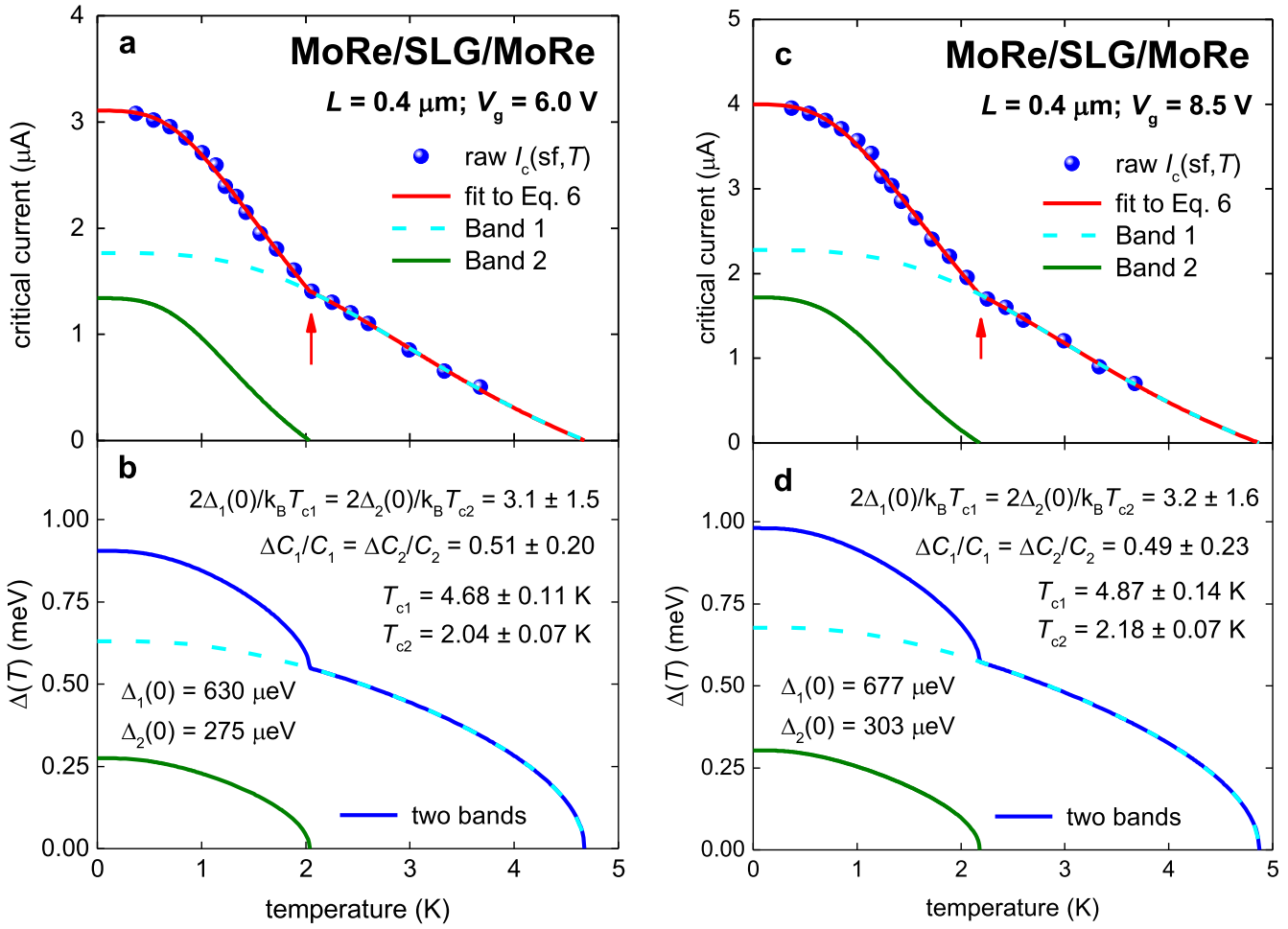

Figure 7. Experimental I_c(sf, T) data from [36] and corresponding fits to the two-decoupled-bands model for a MoRe/SLG/MoRe junction (length of $L = 0.40$ μm) at $V_g = 6.0$ V (a), (b) and $V_g = 8.5$ V (c), (d) together with calculated $\Delta(T)$. (a) $V_g = 6.0$ V. The fit was restricted to $2\Delta_1(0)/k_BT_{c1} = 2\Delta_2(0)/k_BT_{c2}$ and $\Delta C_1/C_1 = \Delta C_2/C_2$. $R_{n1} = 0.56 \pm 0.28$ kΩ, and $R_{n2} = 0.32 \pm 0.16$ kΩ. Fit quality is $R = 0.9937$. (b) $V_g = 6.0$ V. Calculated $\Delta(T)$. (c) $V_g = 8.5$ V. The fit is restricted to $2\Delta_1(0)/k_BT_{c1} = 2\Delta_2(0)/k_BT_{c2}$ and $\Delta C_1/C_1 = \Delta C_2/C_2$. $R_{n1} = 0.48 \pm 0.24$ kΩ, and $R_{n2} = 0.28 \pm 0.14$ kΩ. Fit quality is $R = 0.9923$. (d) $V_g = 8.5$ V. Calculated $\Delta(T)$.

800 mK. Thus, to run the model (equation (5)), we make two restrictions:

1. Values of BCS ratios for each band were forced to be the same:

$$\frac{2\Delta_1(T)}{k_BT_{c,1}} = \frac{2\Delta_2(T)}{k_BT_{c,2}}. \quad (6)$$

2. Values for the relative jump in electronic specific heat at transition temperature, T_c, for both bands were forced to be the same:

$$\left.\frac{\Delta C_1}{C_1}\right|_{T_{c,1}} = \left.\frac{\Delta C_2}{C_2}\right|_{T_{c,2}}. \quad (7)$$

Equations (6) and (7) mean that as the junction length, L, is the same for both bands, then we expect that the superconductivity suppression will be the same for both bands while keeping the same coupling strength for both bands. This assumption cannot in fact be justified in the present paper. More importantly, Di Bernardo *et al* [57] recently showed that there is a possibility for the triggering of a particular pairing type in SLG deposited on $Pr_{2-x}Ce_xCuO_4$. However, in terms of the A–B equation (1) the difference in I_c(sf, T) for different types of pairing will be very difficult to identify in experiments, as the shape of $\Delta(T)$ (see, for instance [58]) differs only marginally for different types of pairing.

Also, we were forced to make some assumptions to restrict the number of parameters as the high-temperature part of the dataset was not available. Moreover, these assumptions do not affect in any way our central conclusions. From all other options we considered the assumptions given by equations (6) and (7) appeared to have the least effect in extracting parameter values for the junction. As we will show later for an analysis of a $Nb/Bi_2Se_3/Nb$ junction (figures 9, 10), for which the experimental dataset was rich enough to run the fit model with all parameters free, the derived free-fitting parameters agree with our assumptions formulated by equations (6) and (7)

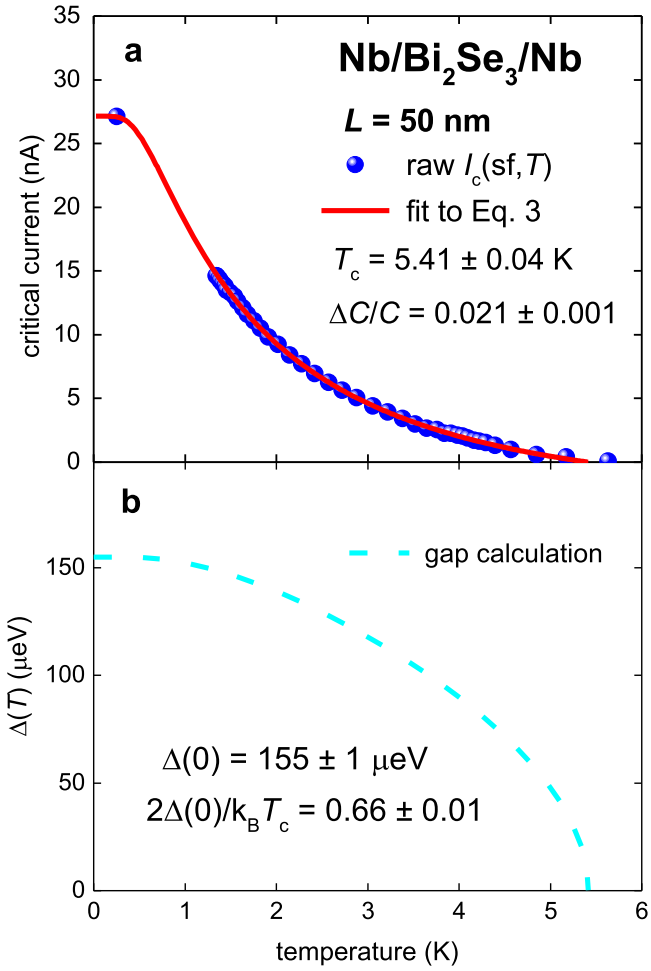

Figure 8. (a) Experimental I_c(sf, T) data from [10] and corresponding fit for Nb/Bi_2Se_3/Nb junction (length of $L = 50$ nm) and (b) calculated $\Delta(T)$. $R_n = 9.00 \pm 0.01\ \Omega$. Fit quality is $R = 0.9994$.

within the deduced uncertainties. To encourage experimentalists to obtain high quality experimental I_c(sf, T) datasets during data collection we have placed our Matlab code for free use online [59]. Thus the experimentalist can immediately analyze their datasets during an experiment and make judgements as to whether to refine their data collection based on, for example, parameter uncertainties.

The fit to equation (5) (with these restrictions) of the experimental I_c(sf, T) dataset for a MoRe/SLG/MoRe junction reported by Calado *et al* [3] is shown in figure 6(a).

The most important result is that the fit converged and clearly shows the presence of two distinct bands (figure 6(a)). The deduced parameters show that the induced superconductivity in the MoRe/SLG/MoRe junction is very robust as the superconductivity is apparently only moderately weakened, taking into account that the junction length is very long, $L = 1.5\ \mu$m. This reflects the very long mean free path $\approx 30\ \mu$m, which was measured in graphene at similar doping level, $n \sim 1.5 \times 10^{12}\ \mathrm{cm}^{-2}$, and even much higher temperature $T = 20$ K [60].

Also, we note that the deduced parameters have acceptable uncertainties. In figure 6(b) we plot the calculated temperature-dependent energy gap for the two-decoupled-bands model:

$$\Delta_{\mathrm{total}}(T) = \Delta_1(T) + \Delta_2(T). \tag{8}$$

It is important to find independent experimental confirmation that SLG in MoRe/SLG/MoRe has a proximity-induced superconducting state with two bands. A recent report published by Borzenets *et al* [7] provided this confirmation and we discuss this now.

3.2.4. Planar MoRe/SLG/MoRe; L = 0.2, 0.4, 1.0, and 2.0 μm. Borzenets *et al* [7] fabricated seven MoRe/SLG/MoRe devices with different junction lengths (in the range of $L = 0.2$–$2.0\ \mu$m) and measured self-field critical currents, I_c(sf, T), at different gate voltages V_g. In figure 7(a) we show I_c(sf, T) datasets and the fit to equation (5) for a relatively short junction with length $L = 0.40\ \mu$m at gate voltages of $V_g = 6.0$ V (original data are in figure 2(b) of [7]). As the I_c(sf, T) measurements were not performed up to temperatures close to T_c, we restrict our model by the same conditions, as before (equations (6) and (7)).

In figure 7(c) we show I_c(sf, T) datasets and the fit to equation (5) for the same junction at a gate voltage of $V_g = 8.5$ V. Derived parameters for this junction obtained at $V_g = 6.0$ and $V_g = 8.5$ V are very comparable with each other (figure 7). This shows that our model can reliably extract fundamental parameters from experimental data in different geometries and different bias settings. The opening of two superconducting gaps in figure 7 is obvious.

I_c(sf, T) datasets for other junctions and gate voltages reported by Borzenets *et al* [7] have similar shapes. However, the currently available experimental data for different junctions were measured at different sets of gate voltages, V_g. Thus, many interesting questions, such as the evolution of fundamental superconducting parameters versus junction length, L, and gate voltage, V_g, remain to be explored in MoRe/SLG/MoRe devices.

3.3. Topological insulator based junctions

We searched for available experimental results for other junctions involving ultra-thin conductors which might exhibit the presence of two superconducting bands. Topological insulators are a possible example since any supercurrent will only be transported on the surface. The two-dimensional nature of the superconducting state in junctions based on Bi_2Se_3 was confirmed by He *et al* [61].

3.3.1. Nb/Bi_2Se_3/Nb junctions; L = 50 nm. Veldhorst *et al* [10] reported the first successful measurements of I_c(sf, T) for superconductor/topological insulator/superconductor junction (in their figure 4(b)) for which the Bi_2Se_3 single crystalline flake has a thickness of 200 nm. They also performed a data fit to the Usadel (dirty limit) and Eilenberger (clean limit) models.

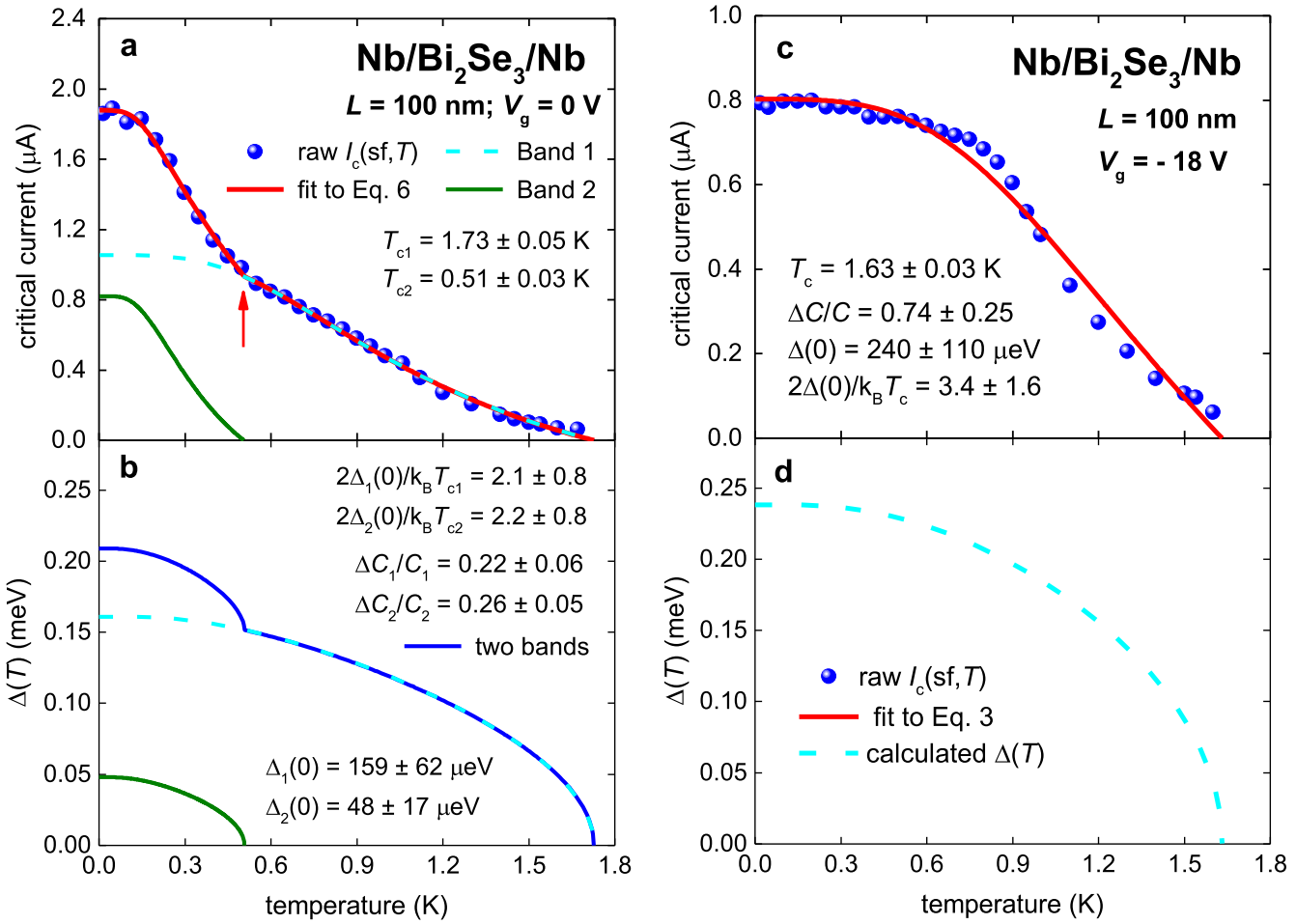

Figure 9. Experimental I_c(sf, T) data from [11] and corresponding fit to the two-decoupled-bands model for $Nb/Bi_2Se_3/Nb$ junction (length of $L = 9$ nm) at $V_g = 0.0$ V (a), (b) and $V_g = -18$ V (c), (d) together with calculated $\Delta(T)$. (a) $V_g = 0.0$ V. $R_{n1} = 0.24 \pm 0.10$ kΩ, $R_{n2} = 0.092 \pm 0.033$ kΩ. Fit quality is $R = 0.9842$. (b) $V_g = 0.0$ V. Calculated $\Delta(T)$. (c) $V_g = -18$ V. $R_{n1} = 0.47 \pm 0.21$ kΩ. Fit quality is $R = 0.7987$. (d) $V_g = -18$ V. Calculated $\Delta(T)$.

Our fit to equation (3) is shown figure 8, and it reveal parameters in the expected range.

3.3.2. Nb/Bi2Se3/Nb junctions; L = 100 nm. Kurter *et al* [11] in their figure 1(b) reported I_c(sf, T) for a two $Nb/Bi_2Se_3/Nb$ junctions with length of $L = 100$ nm, and the Bi_2Se_3 flake has a thickness of 9 nm. In figure 9(a) we show experimental I_c(sf, T) datasets for $Nb/Bi_2Se_3/Nb$ junctions with lengths of $L = 100$ nm at zero applied voltage. The fit to equation (5) was performed for all parameters free as the experimental dataset was suitably rich to carry out this sort of fit.

While the gate voltage of $V_g = -18$ V was applied, the shape of the I_c(sf, T) curve changed [11] as we showed in figure 9(c). This suggests that by varying the doping state of the Bi_2Se_3 topological insulator, one of two superconducting bands can be closed.

The confirmation for this idea is given in figure 9(c), where the experimental I_c(sf, T) dataset was fitted to a single-band model (equation (3)) where within the moderately large uncertainties for the derived parameters, the values correspond to parameters derived by us previously for short-length junctions.

3.3.3. Nb/Bi2Se3/Nb junctions; L = 210 nm. In figure 10, we show data for the case of an S/TI/S junction with length $L = 210$ nm. Kurter *et al* [11] in their figure S1(d) reported I_c(sf, T) for $Nb/Bi_2Se_3/Nb$ junctions with length of $L = 210$ nm, where the Bi_2Se_3 flake has a thickness of 30 nm. We performed a fit of experimental data to equation (5) for a longer $Nb/Bi_2Se_3/Nb$ junction with $L = 210$ nm which is shown in figure 10(a).

Application of a gate voltage of $V_g = -35$ V caused the suppression of smaller gap and, though a residual smaller gap may possibly still be evident in the low-T data, I_c(sf, T) was now fitted to the single-band model as shown in figure 10(b). The derived parameters showed a weakening of superconductivity in comparison with the $Nb/Bi_2Se_3/Nb$ junction having a shorter length (figure 9).

This is a representative example showing that varying the doping state of the material can be an effective tool to open or close superconducting gaps, presumably by shifting the Fermi level and decreasing the number of bands crossing the Fermi level. A remarkable example of applying this technique to transform the insulator (where there is no superconducting gap) to a superconductor with the observation of an entire

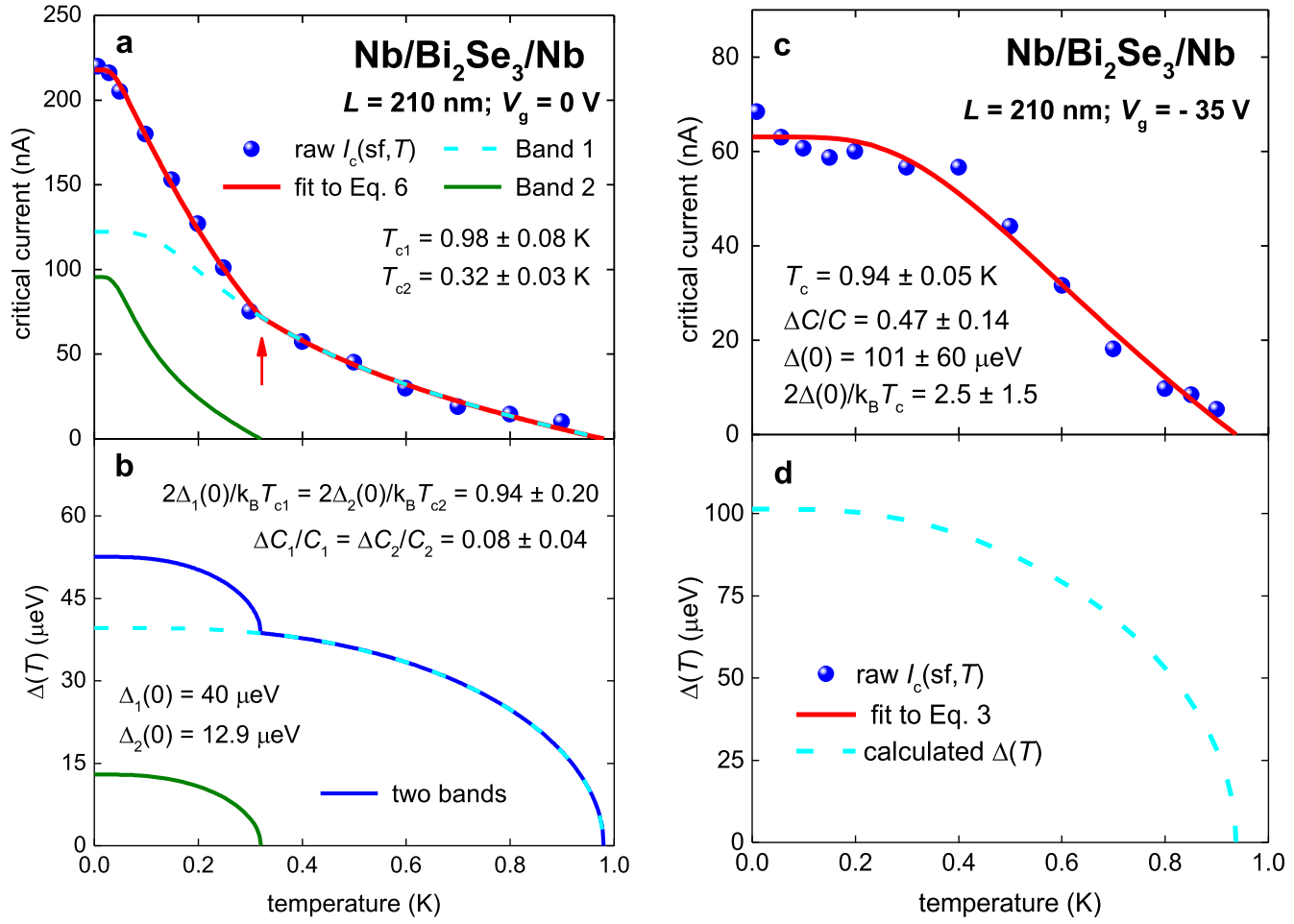

Figure 10. Experimental I_c(sf, T) data from [11] and corresponding fit to the two-decoupled-bands model for Nb/Bi_2Se_3/Nb junction ($L = 30$ nm) at $V_g = 0.0$ V (a), (b) and $V_g = -35$ V (c), (d) together with the calculated $\Delta(T)$. (a) $R_{n1} = 0.51 \pm 0.25$ kΩ, $R_{n2} = 0.213 \pm 0.016$ kΩ. Fit quality is $R = 0.9620$. (b) $V_g = 0.0$ V. Calculated $\Delta(T)$. (c) $V_g = -35$ V. $R_{n1} = 2.5 \pm 1.5$ kΩ. Fit quality is $R = 0.7872$. (d) $V_g = -35$ V. Calculated $\Delta(T)$.

superconducting dome (which means that the superconducting gap continuously changes from zero to the maximum value) was reported by the Ye and Iwasa group [62]. Recently, Dubuis *et al* [63] and Perez-Muñoz *et al* [64] showed that ion gating causes the depletion of oxygen from its specific sites in the unit cell in cuprate superconductors. This atomic rearrangement affects the London penetration depth in cuprates [65] and it should change the superconducting gap amplitude. More recently, Uchiyama *et al* [66] pointed out that there is a difference between the gating and the doping effects in 2D materials, however our results presented in figures 9, 10, where the amplitudes of both superconducting gaps are changing with gate voltage are in good agreement with all experimental results reported by other authors to date in this emerging field. This is also additional support for our previous proposal [51] that the ionic-liquid-gating technique (or more generally, gate voltage doping) can be an effective tool to study the opening and closing of new superconducting gaps in atomically-thin superconductors.

4. Conclusions

Here we have proposed to substitute the analytical expression for the temperature-dependent superconducting energy gap given by Gross *et al* [14] in the A–B equation [12, 13] in order to deduce fundamental superconducting parameters of the junction i.e. $\Delta(0)$, $\Delta C/C$, and T_c from self-field critical currents in S/non-superconductor/S junctions.

We showed that this approach reliably deduced superconducting parameters in Sn/SnO_x/Sn, NbN/MgO/Nb, vdW $NbSe_2$/$NbSe_2$, Al/InAs/Al and PbIn/PbS/PbIn junctions.

We applied this model for vertical graphene- and graphite- Al/vG/Al junctions and show that the derived superconducting parameters exhibit a clear trend of weakening superconductivity with increasing junction length. This weakening (as shown in figures 3–5) is seen most clearly in the relative jump in electronic specific heat at the transition temperature and in the ground-state amplitude of the superconducting energy gap, while the superconducting transition temperature is mostly unaffected.

Also we applied our model for planar Nb/BLG/Nb and MoRe/SLG/MoRe junctions using a two-decoupled-bands model. In the case of SLG we found that the induced superconductivity has two distinct superconducting bands. This was found in two sets of devices fabricated by two independent research groups. These findings are well aligned with the recent result reported by Talantsev *et al* [51] that in atomically-thin Ga, TaS_2, FeSe superconductors and thin films of Nb an additional superconducting gap opens when the film thickness becomes less than the out-of-plane coherence length. Thus, SLG-based proximity devices appear to demonstrate the same phenomenon with two superconducting gaps present and certainly the graphene thickness is well below the out-of-plane coherence length of any superconductor that might be used as a proximity-effect electrode. More experimental studies are required to identify the thickness/length/gate-voltage dependence of this two-band superconductivity in S/G/S junctions.

A two superconducting band state was also discovered in Nb/Bi_2Se_3/Nb junctions and we interpreted earlier experimental results reported by other authors in terms of a doping-induced gap closing in a topological insulator. As the topological insulator is able to carry a supercurrent only on the surface, again, the effective thickness of the superconducting layer is more likely to be atomically thin and less than the relevant coherence length—consistent with our two superconducting band hypothesis.

Certainly the band structure changes in these quantum-confined systems however we emphasize that this is not merely the consequent magnification and modulation of the density of states that can arise in such circumstances [67] and which can enhance the superconducting gap but we observe the opening of an *additional* gap. This awaits explanation.

Acknowledgments

The authors would like to thank Dr S Goswami and Professor L M K Vandersypen (Kavli Institute of Nanoscience, Delft University of Technology, The Netherlands) for providing raw experimental critical current data for the MoRe/SLG/MoRe device, and Professor H-J Lee (Pohang University of Science and Technology, Republic of Korea) for supporting information about vertical graphene-based junctions analyzed in this work.

EFT acknowledges support from the Marsden Fund of New Zealand grant number VUW1608, a Victoria University of Wellington PBRF support grant number 215637, and a Victoria University of Wellington travel grant award number 3719. JLT thanks the Marsden Fund and the MacDiarmid Institute for Advanced Materials and Nanotechnology for financial support.

ORCID iDs

E F Talantsev https://orcid.org/0000-0001-8970-7982

References

[1] Heersche H B, Jarillo-Herrero P, Oostinga J B, Vandersypen L M K and Morpurgo A F 2007 Bipolar supercurrent in graphene *Nature* **446** 56–9
[2] Du X, Skachko I and Andrei E Y 2008 Josephson current and multiple Andreev reflections in graphene SNS junctions *Phys. Rev.* B **77** 184507
[3] Calado V E *et al* 2015 Ballistic Josephson junctions in edge-contacted graphene *Nat. Nanotechnol.* **10** 761–4
[4] Lee G H, Kim S, Jhi S-H and Lee H-J 2015 Ultimately short ballistic vertical graphene Josephson junctions *Nat. Commun.* **6** 6181
[5] Ben Shalom M *et al* 2016 Quantum oscillations of the critical current and high-field superconducting proximity in ballistic graphene *Nat. Phys.* **12** 318–22
[6] Amet F *et al* 2016 Supercurrent in the quantum Hall regime *Science* **352** 966–9
[7] Borzenets I V *et al* 2016 Ballistic graphene Josephson junctions from the short to the long junction regimes *Phys. Rev. Lett.* **117** 237002
[8] Island J O, Steele G A, van der Zant H S J and Castellanos-Gomez A 2016 Thickness dependent interlayer transport in vertical MoS_2 Josephson *2d. Mater.* **3** 031002
[9] Zhu M J *et al* 2017 Edge currents shunt the insulating bulk in gapped graphene *Nat. Commun.* **8** 14552
[10] Veldhorst M *et al* 2012 Josephson supercurrent through a topological insulator surface state *Nat. Mater.* **11** 417–21
[11] Kurter C, Finck A D K, Hor Y S and Van Harlingen D J 2015 Evidence for an anomalous current–phase relation in topological insulator Josephson junctions *Nat. Commun.* **6** 7130
[12] Ambegaokar V and Baratoff A 1963 Tunneling between superconductors *Phys. Rev. Lett.* **10** 486–9
[13] Ambegaokar V and Baratoff A 1963 Errata: tunneling between superconductors *Phys. Rev. Lett.* **11** 104
[14] Gross F *et al* 1986 Anomalous temperature dependence of the magnetic field penetration depth in superconducting UBe_{13} *Z. Phys.* B **64** 175–88
[15] Josephson B D 1962 Possible new effects in superconductive tunneling *Phys. Lett.* **1** 251–3
[16] Likharev K K 1979 Superconducting weak links *Rev. Mod. Phys.* **51** 101–59
[17] Kulik I and Omelyanchuk A 1978 The Josephson effect in superconducting constrictions: microscopic theory *J. Phys. Coll.* **39** 546–7
[18] Delin K A and Kleinsasser A W 1996 Stationary properties of high-critical-temperature proximity effect Josephson junctions *Supercond. Sci. Technol.* **9** 227–69
[19] Golubov A A, Kupriyanov M Y and Il'ichev E 2004 The current-phase relation in Josephson junctions *Rev. Mod. Phys.* **76** 411–69
[20] Eilenberger G 1968 *Z. Phys.* **214** 195–213
[21] Usadel K D 1970 Generalized diffusion equation for superconducting alloys *Phys. Rev. Lett.* **25** 507–9
[22] Brinkman A and Golubov A A 2000 Coherence effects in double-barrier Josephson junctions *Phys. Rev.* B **61** 11297–300
[23] Nanda G *et al* 2017 Current–phase relation of ballistic graphene Josephson junctions *Nano Lett.* **17** 3396–401
[24] Foley C P, Lam S, Sankrithyan B and Wilson Y 1997 The effects of step angle on step edge Josephson junctions on MgO *IEEE Trans. Appl. Supercond.* **7** 3185–8
[25] Du J, Macfarlane J C, Leslie K E, Foley C P, Hellicar A D, Li L and Hanham S M 2009 High-T_c superconducting step-edge Josephson junction detector for terahertz imaging *Proc 2009 Int. Conf. Applied Superconductivity Electromagnetic Devices—ASEMD 2009 (Chengdu, China, 25–27 September 2009)* pp 127–30

[26] Kleiner R, Steinmeyer F, Kunkel G and Mueller P 1992 Intrinsic Josephson effects in $Bi_2Sr_2CaCu_2O_8$ single crystals *Phys. Rev. Lett.* **68** 2394–7

[27] Kleiner R and Muller P 1994 Intrinsic Josephson effects in high-T_c superconductors *Phys. Rev.* B **49** 1327

[28] Matsuda Y, Gaifullin M B, Kumagai K, Kadowaki K and Mochiku T 1995 Collective Josephson plasma resonance in the vortex state of $Bi_2Sr_2CaCu_2O_8$ *Phys. Rev. Lett.* **75** 4512–5

[29] Warburton P A *et al* 2004 Josephson fluxon flow and phase diffusion in thin-film intrinsic Josephson junctions *J. Appl. Phys.* **95** 4941–8

[30] Kizilaslan O, Truccato M, Simsek Y, Aksan M A, Koval Y and Müller P 2016 *Supercond. Sci. Technol.* **29** 065013

[31] Mueller P, Koval Y, Lazareva Y, Steiner C, Wurmehl S, Buechner B, Stuerzer T and Johrendt D 2017 *C*-axis transport of pnictide superconductors *Phys. Status Solidi* b **254** 1600157

[32] Anderson J T and Goldman A M 1969 Thermal fluctuations and the Josephson supercurrent *Phys. Rev. Lett.* **23** 128–31

[33] Wolf E L 1985 *Principles of Electron Tunneling Spectroscopy* (New York: Oxford University Press) p 524

[34] Bardeen J, Cooper L N and Schrieffer J R 1957 Theory of superconductivity *Phys. Rev.* **108** 1175–204

[35] Padamsee H, Neighbor J E and Shiffman C A 1973 Quasiparticle phenomenology for thermodynamics of strong-coupling superconductors *J. Low Temp. Phys.* **12** 389–411

[36] Shoji A, Aoyagi M, Kosaka S, Shinoki F and Hayakawa H 1985 Niobium nitride Josephson tunnel junctions with magnesium oxide barriers *Appl. Phys. Lett.* **46** 1098–2100

[37] Kihlstrom K E, Simon R W and Wolf S A 1986 Tunneling $\alpha^2 F(\omega)$ from sputtered thin-film NbN *Phys. Rev.* B **32** 1843(R)–45(R)

[38] Geibel C, Rietschel H, Junod A, Pelizzone M and Muller J 1985 Electronic properties, phonon densities of states and superconductivity in $Nb_{1-x}V_xN$ *J. Phys. F: Met. Phys.* **15** 405–16

[39] Abay S *et al* 2014 Charge transport in InAs nanowire Josephson junctions *Phys. Rev.* B **89** 214508

[40] Yabuki N *et al* 2016 Supercurrent in van der Waals Josephson junction *Nat. Commun.* **7** 10616

[41] Weber F, Rosenkranz S, Heid R and Said A H 2016 Superconducting energy gap of 2H–$NbSe_2$ in phonon spectroscopy *Phys. Rev.* B **94** 140504(R)

[42] Morris R C and Coleman R V 1973 Tunneling measurement of the superconducting energy gap in $NbSe_2$ *Phys. Lett.* A **43** 11–2

[43] Pescaglini A *et al* 2011 Role of contact material on transport properties of InAs nanowire Josephson junctions *AIP Conf. Proc.* **1399** 281–2

[44] Abay S *et al* 2012 High critical-current superconductor-InAs nanowire-superconductor junctions *Nano Lett.* **12** 5622–5

[45] Kim B K and Doh Y J 2016 Switching current distributions in InAs nanowire Josephson junctions *J. Korean Phys. Soc.* **69** 349–53

[46] Carbotte J P 1990 Properties of boson-exchange superconductors *Rev. Mod. Phys.* **62** 1027–157

[47] Kim B-K *et al* 2017 Strong superconducting proximity effects in PbS semiconductor nanowires *ACS Nano* **11** 221–6

[48] Lacquaniti V, De Leo N, Fretto M, Sosso A and Belogolovskii M 2010 Nb/Al–AlO_x–Nb superconducting heterostructures: a promising class of self-shunted Josephson junctions *J. Appl. Phys.* **108** 093701

[49] Won H and Maki K 1994 *d*-wave superconductor as a model of high-T_c superconductors *Phys. Rev.* B **49** 1397–402

[50] Natterer F D, Ha J, Baek H, Zhang D, Cullen W G, Zhitenev N B, Kuk Y and Stroscio J A 2016 Scanning tunneling spectroscopy of proximity superconductivity in epitaxial multilayer graphene *Phys. Rev.* B **93** 045406

[51] Talantsev E F, Crump W P, Island J O, Xing Y, Sun Y, Wang J and Tallon J L 2017 On the origin of critical temperature enhancement in atomically thin superconductors *2d. Mater.* **4** 025072

[52] Zhang W-H *et al* 2014 Direct observation of high-temperature superconductivity in one-unit-cell FeSe films *Chin. Phys. Lett.* **31** 017401

[53] Navarro-Moratalla E *et al* 2016 Enhanced superconductivity in atomically thin TaS_2 *Nat. Commun.* **7** 11043

[54] Zhang H-M *et al* 2015 Detection of a superconducting phase in a two-atom layer of hexagonal Ga film grown on semiconducting GaN(0001) *Phys. Rev. Lett.* **114** 107003

[55] Xing Y *et al* 2015 Quantum Griffiths singularity of superconductor-metal transition in Ga thin films *Science* **350** 542–5

[56] Rusanov A Y, Hesselberth M B S and Aarts J 2004 Depairing currents in superconducting films of Nb and amorphous MoGe *Phys. Rev.* B **70** 024510

[57] Di Bernardo A *et al* 2017 P-wave triggered superconductivity in single-layer graphene on an electron-doped oxide superconductor *Nat. Commun.* **8** 14024

[58] Poole P P, Farach H A, Creswick R J and Prozorov R 2014 *Superconductivity* 3rd edn (Amsterdam: Elsevier) ch 11 p 459

[59] Crump W P and Talantsev E F 2017 Free-upload software: https://github.com/WayneCrump/

[60] Wang L *et al* 2013 One-dimensional electrical contact to a two-dimensional material *Science* **342** 614–7

[61] He Q L *et al* 2014 Two-dimensional superconductivity at the interface of a Bi_2Te_3/FeTe heterostructure *Nat. Commun.* **5** 4247

[62] Ye J T, Zhang Y J, Akashi R, Bahramy M S, Arita R and Iwasa Y 2012 Superconducting dome in a gate tuned band insulator *Science* **338** 1193–6

[63] Dubuis G, Yacoby Y, Zhou H, He X, Bollinger A T, Pavuna D, Pindak R and Božović I 2016 Oxygen displacement in cuprates under ionic liquid field-effect gating *Sci. Rep.* **6** 32378

[64] Perez-Muñoz A M *et al* 2017 In operando evidence of deoxygenation in ionic liquid gating of $YBa_2Cu_3O_{7-x}$ *Proc. Natl Acad. Si.* **114** 215–20

[65] Fête A, Rossi L, Augieri A and Senatore C 2016 Ionic liquid gating of ultra-thin $YBa_2Cu_3O_{7-x}$ films *Appl. Phys. Lett.* **109** 192601

[66] Uchiyama T, Goto H, Akiyoshi H, Eguchi R, Nishikawa T, Osada H and Kubozono Y 2017 Difference in gating and doping effects on the band gap in bilayer graphene *Sci. Rep.* **7** 11322

[67] Shanenko A A, Croitoru M D, Mints R G and Peeters F M 2007 New Andreev-type states in superconducting nanowires *Phys. Rev. Lett.* **99** 067007